Plasmodium falciparum Exports the Golgi Marker Sphingomyelin Synthase into a Tubovesicular Network in the Cytoplasm of Mature Erythrocytes

Heidi G. Elmendorf and Kasturi Haldar

Department of Microbiology and Immunology, Stanford University School of Medicine, Stanford, California 94305-5402

Abstract. This work describes two unusual features of membrane development in a eukaryotic cell. (*a*) The induction of an extensive network of tubovesicular membranes by the malaria parasite *Plasmodium falciparum* in the cytoplasm of the mature erythrocyte, and its visualization with two ceramide analogues C_5-DMB-ceramide and C_6-NBD-ceramide. "Sectioning" of the infected erythrocytes using laser confocal microscopy has allowed the reconstruction of detailed three-dimensional images of this novel membrane network. (*b*) The stage-specific export of sphingomyelin synthase, a biosynthetic activity concentrated in the Golgi of mammalian cells, to this tubovesicular network. Evidence is presented that in the extracellular merozoite stage the parasite retains sphingomyelin synthase within its plasma membrane. However, intracellular ring- and trophozoite-stage parasites export a substantial fraction (~26%) of sphingomyelin synthase activity to membranes beyond their plasma membrane. Importantly we do not observe synthesis of new enzyme during these intracellular stages. Taken together these results strongly suggest that the export of this classic Golgi enzyme is developmentally regulated in *Plasmodium*. We discuss the significance of this export and the tubovesicular network with respect to membrane development and function in the erythrocyte cytosol.

PLASMODIUM *falciparum* is a protozoan parasite responsible for the most virulent form of human malaria. Its asexual life cycle begins when the extracellular merozoite stage invades the mature erythrocyte. Here the parasite develops inside a parasitophorous vacuole during a 48-h life cycle through the ring (0–24 h after invasion), trophozoite (24–36 h), and schizont (36–48 h) stages; these stages are distinguished by specific morphological and biosynthetic characteristics. The mature erythrocyte lacks all organelles and is incapable of de novo protein and lipid synthesis. The intracellular parasite extensively modifies both biochemical and ultrastructural properties of the red cell. These modifications are thought to be essential to the parasite's survival in this quiescent host cell. A very striking alteration is the development of new membrane structures in the infected erythrocyte cytoplasm.

These membranes were first seen as individual compartments by transmission electron microscopy (Langreth et al., 1978; for review see Atkinson and Aikawa, 1990). Slender cisternae (0.2–0.4 μm in length; Maurer's clefts) and large loops (0.1–1 μm in diameter) have been described as distinct structures in the erythrocyte cytoplasm. Immunolocalization studies by Stenzel and Kara (1989) suggest that proteins exported to loops bud from the surface of the parasitophorous vacuole. Parasite proteins in the cisternae are also clearly sorted away from those in the large vesicles (Coppel et al., 1986; Howard et al., 1987*b*; Taylor et al., 1987; Hui and Siddiqui, 1988; Etzion and Perkins, 1989; Li et al., 1991). On the basis of these data and the morphology of the cisternal membranes, it has been suggested that intraerythrocytic compartments may act as secretory organelles (Howard et al., 1987*a*; Barnwell, 1990) and that the infected erythrocyte cytosol supports vesicular transport at the vacuolar and intraerythrocytic surfaces.

Labeling of *P. falciparum*–infected erythrocytes with fluorescent phospholipid and sphingolipid analogues again reveals membrane structures in the erythrocyte cytoplasm (Grellier et al., 1991; Haldar et al., 1991; Pouvelle et al., 1991; Gormley et al., 1992; Haldar and Uyetake, 1992). With the lipid probes, however, the structures appear quite large, consisting of tubular and vesicular elements. Specifically, we found that in cells labeled with C_6-NBD-ceramide (*N*-[7-(4-nitrobenzo-2-oxa-1,3-diazole)]-6-aminocaproyl-D-erythro-sphingosine) large membrane elements were prominent in the erythrocyte cytosol. Surprisingly, photoconversion of the fluorescent sphingolipid to a diaminobenzidine prod-

Address all correspondence to K. Haldar, Department of Microbiology and Immunology, Stanford University School of Medicine, Stanford, CA 94305-5402.

H. G. Elmendorf's present address is Department of Biology, Phillips Academy, Andover, MA 01810.

uct resulted in the presence of electron dense precipitates in the loops and cisternae (Haldar et al., 1991), demonstrating that the cisternae and loops seen by transmission electron microscopy were the same as the large tubules and vesicles labeled by C_6-NBD-ceramide. Due to limitations in microscopic technique, we could not resolve whether the fluorescent membranes detected by C_6-NBD-ceramide were discrete entities (i.e., clusters of cisternae) or were connected (i.e., tubules) in the erythrocyte cytosol. In recent studies by Elford and Ferguson (1993), scanning electron micrographs of parasites released from their erythrocyte hosts, show long tubular and vesicular structures extending from the surface of the parasite. However, it remained unclear whether these structures were generated by the process of releasing the parasite or represented a true network of the cisternae and loops detected by transmission electron microscopy. Thus although membrane structures assemble in the erythrocyte cytoplasm, their precise morphologies and whether they are discrete products of vesiculation or continuous (albeit complex) extensions of the vacuolar surface in live infected erythrocytes, remain unknown.

The development of intraerythrocytic membranes (whether discrete or continuous in nature) has suggested that the parasite secretory apparatus has novel features. The addition of oligosaccharides N-linked to proteins is almost universally detected in eukaryotic cells. It appears to be absent in *Plasmodium* (Dieckmann-Schuppert et al., 1992), suggesting one unusual feature: its significance is unknown. Many other Golgi enzymes responsible for posttranslational protein modifications are also not apparent: sialyltransferase (Schauer et al., 1984), galactosyltransferase, and *N*-acetylglucosamine transferase (Crary, J., W.-l. Li, and K. Haldar, unpublished data). Despite the lack of N-linked glycosylation we find that the parasite's Golgi is compartmentalized (Elmendorf and Haldar, 1993). Surprisingly, a malarial ERD2 homologue and sphingomyelin synthase (ascribed to the *cis*-Golgi in mammalian cells) are localized in distinct compartments in the parasite. The perinuclear distribution of sphingomyelin synthase is unaffected by brefeldin A, indicating that the dynamics of this compartment in the plasmodial Golgi is distinct from that in mammalian cells (Elmendorf and Haldar, 1993).

In a number of cultured mammalian cell lines, fluorescent ceramide analogues accumulate in the Golgi of live cells. These probes therefore provide a vital stain for the Golgi complex and have been used to show that ceramide is metabolized to sphingomyelin in this organelle (Lipsky and Pagano, 1985; Pagano et al., 1991). The most recent subcellular fractionation studies also indicate that the lumen of the *cis*- and *medial*-Golgi cisternae are the major sites of sphingomyelin biosynthesis from ceramide (Futerman et al., 1990; Jeckel et al., 1990). In a particularly rigorous study using well-characterized fraction from rat liver ~87% of the activity was found in the Golgi (Futerman et al., 1990). The remaining ~13% was at the plasma membrane, suggesting the presence of a second (albeit minor) site of sphingomyelin synthase activity in cells. Other studies, however, have indicated that a greater fraction of sphingomyelin synthase activity is at the plasma membrane (Quinn and Allan, 1992; Kallen et al., 1993). These discrepancies have raised some controversy concerning the distribution of the enzyme and the possibility that there may be two forms of the enzyme in cells. Sphingomyelin newly synthesized in the Golgi is exported to the plasma membrane and subsequently internalized in components of the endocytic pathway (Koval and Pagano, 1991). It is believed that the sphingolipid composition of the Golgi plays an important role in the secretory functions of the compartment (van Meer, 1989; Pagano, 1990). This proposal is supported by data showing that the inhibition of sphingomyelin synthesis correspondingly inhibits protein trafficking, suggesting a link between sphingolipid synthesis and protein and lipid transport (Rosenwald et al., 1992).

In this paper, we use two fluorescent ceramide analogues, C_5-DMB-ceramide (*N*-[5-(5,7-dimethylBODIPY)-1-pentanoyl]-D-erythro-sphingosine) and C_6-NBD-ceramide in both microscopic and biochemical studies to define the location of sphingolipid accumulation and metabolism in *P. falciparum*. We provide evidence for a reticulum of intraerythrocytic membrane (designated as a tubovesicular membrane network [TVM]),[1] rather than separated membrane structures in intact, infected erythrocytes and show that it contains sites of ceramide and sphingomyelin accumulation. Previous work by our laboratory demonstrated the conversion of C_6-NBD-ceramide to C_6-NBD-sphingomyelin by a parasite sphingomyelin synthase. While we recently localized this secretory enzyme to a perinuclear region within the intraerythrocytic parasite (Elmendorf and Haldar, 1993) we did not directly compare its distribution at different stages of parasite development. We show here that in extracellular merozoites the enzyme is retained completely within the parasite and this stage of the parasite is highly enriched for the enzyme. However, in the intracellular ring and trophozoite stages the parasite exports a fraction of the activity beyond the parasite plasma membrane. In contrast, the malarial homologue of ERD2, a resident protein of the Golgi, is retained within the parasite at all stages of the asexual life cycle (Elmendorf and Haldar, 1993). This indicates a selective, well-orchestrated rearrangement of sphingomyelin synthase in the *P. falciparum*–infected erythrocyte, and we speculate on possible roles for the exported enzyme in the biogenesis and function of the intraerythrocytic membranes.

Materials and Methods

Culturing *P. falciparum* FCR-3/A_2

The clonal line of *P. falciparum* FCR-3/A_2 (Trager et al., 1981) was cultured in vitro according to a modification of the method of Trager and Jensen (Trager and Jensen, 1976; Haldar et al., 1985). The culture media contained RPMI-1640 (GIBCO BRL, Gaithersburg, MD) supplemented with 25 mM Hepes, pH 7.4, 11 mM glucose, 92 μM hypoxanthine, 0.18% $NaHCO_3$, 25 μg/ml gentamicin, and 10% AB^+ human serum (Gemini Bio-Products, Calabasas, CA). The parasites were grown in A^+ red blood cells (0–4 wk old) at 2.5–5% hematocrit. Parasite cultures were synchronized to within 10 h by separation of the early and late stages over Percoll gradients and the subsequent separate reincubation of these stages in culture.

Labeling of Infected Erythrocytes for Confocal Microscopy

Infected erythrocytes were washed free of serum three times in RPMI-1640 and resuspended at 1×10^8 cells/ml in RPMI-1640 containing 2 mg/ml defatted BSA (Sigma Chemical Co., St. Louis, MO) and 20 μM C_5-DMB-ceramide (Molecular Probes Inc., Eugene, OR). Cells were labeled for 60

1. *Abbreviations used in this paper*: EM, erythrocyte membrane; TVM, tubovesicular membrane.

min at 20 or 37°C, washed three times in RPMI-1640, and viewed live or after light fixation in 0.05% glutaraldehyde. Cells were viewed on a custom-made laser confocal microscope designed by S. J. Smith (Department of Molecular and Cell Physiology, Stanford University). Images were taken at 400-nm intervals along the z-axis. Raw confocal data was processed using Adobe Photoshop software. Three-dimensional image analysis was performed on raw confocal data using ImageSpace software (Molecular Dynamics, Inc., Sunnyvale, CA) as modified by W. Jung (Cell Sciences Imaging Facility, Stanford University).

Back-extraction of Infected Erythrocytes

Infected erythrocytes were washed and labeled as above using C_6-NBD-ceramide (Molecular Probes Inc.). After labeling, the cells were washed three times in RPMI-1640, back-extracted three times at 0°C for 20 min each in 1 ml RPMI-1640 containing 7 mg/ml defatted BSA, and subsequently fixed as described above. Aliquots of cells were removed and analyzed by lipid extraction and thin layer chromatography to confirm the efficiency of ceramide extraction. Cells were viewed as above.

Preparation of Merozoites

Merozoites were prepared by the method of Mrema et al. (1982). Cultures were first synchronized in two steps to a 4-h span in the life cycle. Schizonts purified over Percoll gradients were subcultured into fresh erythrocytes and monitored hourly for the presence of rings. 4 h after the first appearance of ring stages the cultures were treated with 5% sorbitol, a treatment which kills mature schizonts but not the ring infected erythrocytes. These cultures were allowed to mature, and 44h+ schizonts were purified away from uninfected erythrocytes over 65% Percoll in RPMI 1640 and incubated at 0.5 to 1% hematocrit in RPMI-1640 containing 10% human serum at 37°C. At 2-h intervals, the cultures were centrifuged at 500 *g* for 5 min. The culture supernatants, enriched for merozoites, were sequentially filtered through 3.0- and 1.2-μm filters. The purified merozoites in the filtrate were collected by centrifugation and washed twice in ice cold RPMI-1640. To estimate yields a small aliquot was diluted into a known number of red cells, the preparation was giemsa stained and the ratio of merozoites to red cells was determined. No schizonts were detected in the preparations despite exhaustively examining 10,000–50,000 cells in thick smears. Assuming that each schizont produced 16 daughter merozoites, the net yield varied between 25–35% of the starting material. The protein content of the samples was measured by the Bio Rad method.

Assaying Sphingomyelin Synthase Activity in Merozoites, Ring-, Trophozoite-, and Schizont-infected Erythrocytes

Equal numbers of merozoites or infected erythrocytes at the ring, trophozoite, or schizont stage were incubated with 10 μM C_6-NBD-ceramide or (C_5-DMB-ceramide) in either RPMI-1640 or PBS at 37°C for 15, 30, or 60 min, and the samples were immediately extracted for lipid analysis.

To determine the effects of protein synthesis inhibitors on sphingomyelin synthase activity, ring-, trophozoite-, and schizont-infected red cells were incubated with 100 μg/ml cycloheximide in RPMI-1640 for 3 h. The cells were collected by centrifugation and labeled with C_6-NBD-ceramide as described (Haldar et al., 1991) for 30 min at 37°C in the continued presence of cycloheximide. In mock incubations both the pretreatment and the labeling were carried out in RPMI-1640 alone. The effects of cycloheximide on protein synthesis and parasite growth were determined as described by Elmendorf et al. (1992).

To assay for the distribution of sphingomyelin synthase in merozoites, incubations containing 100 μg/ml protein in 100 μl PBS were used. Where indicated Proteinase K was added at a final concentration of 100 μg/ml. CHAPS (Pierce, Rockford, IL) and saponin were used at 0.1% wt/vol and 1% wt/vol, respectively. The substrates C_6-NBD-ceramide or C_5-DMB-ceramide were added last at a final concentration of 10 μM and samples were incubated for 30 min at 37°C. The reaction was stopped by the addition of 1 mM PMSF and chilling the samples on ice. Lipids were immediately extracted and analyzed by thin layer chromatography.

Isolation of Released P. falciparum Ring and Trophozoite Stage Parasites and the Erythrocyte Membrane/TVM

Released parasites were prepared as described previously (Elmendorf et al., 1992). Briefly, cultures at the late ring and trophozoite stages were washed once, resuspended to 6% hematocrit in homogenization buffer (65 mM sucrose, 15 mM K^+EDTA, 85 mM Hepes, pH 7.4, 0.3 mM DTT, 1 mg/ml BSA) at 2°C, and subjected to 10–15 passages in a stainless-steel ball homogenizer (internal bore diameter, 0.2500 inches; ball diameter, 0.2494 inches). The homogenate was diluted 10-fold into buffer A (95 mM K^+OAc^-, 15 mM Na^+EDTA, 6.5 mM sucrose, 20 mM Hepes, pH 7.4, 0.3 mM DTT, 1 mg/ml BSA, 8 mg ml^{-1} glucose) and intact cells were collected by centrifugation (2,000 *g*, 10 min, 0°C). The homogenate was processed as described below. The cell pellet was resuspended in buffer A containing a 1× vitamin/amino acid mix from a methionine-minus RPMI 1640 Select Amine Kit, layered onto a 10/40% Percoll gradient in buffer A, and centrifuged at 2,000 *g* for 10 min at 0°C. The 10/40% interface was collected and washed three times in buffer A plus the vitamin/amino acid mix.

The cell-free homogenate was loaded on a 2 M sucrose cushion made up in buffer A (27 ml of homogenate/10 ml of sucrose cushion in Beckman Ultra-Clear Tubes, 1 × 3.5 in) and centrifuged at 100,000 *g* for 60 min in 2°C in a Beckman SW 28 rotor (Beckman Instruments, Inc., Fullerton, CA). The membrane interfaces were pooled and diluted into buffer A as needed.

Labeling of Released Ring and Trophozoite Parasites with C_6-NBD-Ceramide for Microscopy

Released parasites were resuspended at 5 × 10^7 cells/ml in buffer B containing 2 mg/ml defatted BSA and 20–40 μM C_6-NBD-ceramide. Parasites were labeled for 30 min at 37°C and washed three times in buffer B containing 2 mg/ml defatted-BSA after labeling. Bisbenzamide dye (Hoechst 33258) was included in the final wash at a concentration of 5 μg/ml. Samples were viewed using an Olympus BO71 epi-fluorescence microscope with a PM-10AD photomicrographic adapter. C_6-NBD-ceramide labeling was viewed with fluorescein filters. Bisbenzamide labeling was viewed with UV filters. Fluorescence micrographs were typically exposed for 2–8 s using Kodacolor 400 ASA film (Eastman Kodak Co., Rochester, NY); corresponding light micrographs were typically exposed for 1–2 s.

Comparison of Sphingomyelin Synthase Activity in Infected Erythrocytes, Released Rings, and Trophozoites, and Isolated Erythrocyte Membrane/TVM Fractions

Cultures at 20–35% late ring and trophozoite stage parasites were used. Infected erythrocytes were homogenized and released parasite and membrane fractions collected as described above. An aliquot of infected erythrocytes from the same culture was washed three times in RPMI-1640. Parasite equivalents of infected erythrocytes, released parasites, and the membrane fraction were used. Cell and membrane fractions were labeled for 60 min at 37°C in 10 μM C_6-NBD-ceramide in 1–2 ml of appropriate buffer, buffer A for released parasite and membrane fractions, and RPMI-1640 for infected erythrocytes. Fractions were immediately extracted for lipid analysis.

We used two methods to estimate the contamination of the erythrocyte membrane (EM)/TVM fraction by parasite membranes. (*a*) In the first method, the extent of parasite breakage during homogenization was used to calculate the possible contamination by the following equation:

[(Δ number of parasites before and after release)/
(parasite number before release)] ×
sphingomyelin synthase activity of released parasites =
activity in the EM/TVM fraction attributable to contamination.

(Total activity in EM/TVM fraction) − (Activity from contamination) =
sphingomyelin synthase activity exported to the EM/TVM fraction.

(*b*) In the second method, we determined the levels of a parasite homologue of ERD2 (PfERD2) and the major merozoite surface protein (MSP1), markers for the parasite Golgi and plasma membrane, respectively, in the EM/TVM fraction.

Extraction and Analysis of Lipids by Thin Layer Chromatography and Spectrophotometry

Cellular lipids were extracted by a modification of the method of Bligh and Dyer (1959). Four volumes of water-saturated chloroform:methanol (2:1) were added to each sample and vortexed for 30 s. Organic and aqueous

phases were separated by centrifugation for 3 min at 500 *g*. The aqueous phase was re-extracted twice more with four volumes of water-saturated chloroform:methanol. Organic phases containing lipids were pooled, dried under nitrogen gas, and analyzed by thin layer chromatography (TLC) as described previously (Haldar et al., 1991). HPTLC plates (without fluorescent indicator) were obtained from Darmstadt Merck (Drieich, Germany) and Whatman (Clifton, NJ). Quantitation was performed by scraping of fluorescent areas and elution of lipid in ethanol; samples were read on a Perkin-Elmer 650-10S Fluorescence Spectrophotometer (Perkin-Elmer Corp., Norwalk, CT). To convert relative fluorescence units to moles of sphingomyelin, a standard curve was generated using commercially available NBD-sphingomyelin.

Gel Electrophoresis and Immunoblotting

Samples were solubilized in SDS sample buffer, electrophoresed on 7.5% SDS-PAGE gels, and transferred for 12 h at 27 V to nitrocellulose paper. Nitrocellulose was blocked in 5% milk in PBS for 1 h. The filters were incubated with primary antibodies to MSP1, PfERD2, or the 45-kD protein for 2 h at 37°C, followed by three washes in 1% milk, 0.05% Tween-20 in PBS, appropriate second antibody conjugated to peroxidase (Sigma Chemical Co.) (diluted 1:1,000 in 5% milk in PBS) for 2 h at 37°C, three washes in 1% milk, 0.05% Tween-20 in PBS, followed by detection with ECL detection kit (diluted 2:5 in PBS) (Amersham Corp., Arlington Heights, IL) or LumiGlo (Kirkegaarde and Perry Laboratories, Inc., Gaithersburg, MD). Anti-MSP1 and -PfERD2 were diluted 1:500 in 5% milk in PBS and probed with goat anti-rabbit IgG. The monoclonal antibody LWLI raised to the 45-kD protein was diluted 1:1,000 and probed with goat anti-mouse IgA, G, M.

Results

Visualization of Intraerythrocytic Tubular/Vesicular Structures Elaborated by the Intracellular Parasites in the Erythrocyte

Infected erythrocytes were labeled by incubation with 20 μM C_5-DMB-ceramide, stabilized by light fixation in 0.05% glutaraldehyde, and viewed by confocal microscopy. Incubation at 37°C consistently resulted in the labeling of the periphery of the parasite, an arc within the parasite, and tubular and vesicular membranes (TVM) within the erythrocyte. Fig. 1 shows 400-nm serial sections along the z-axis through a single erythrocyte containing a trophozoite stage parasite; parasite stage was determined by bright field analysis of the size of the parasite relative to the red cell and the presence of hemozoin in its digestive vacuole. In Fig. 1, the erythrocyte membrane is the outer circle, and the parasite is the inner circle at the right. The periphery of the parasite is in-

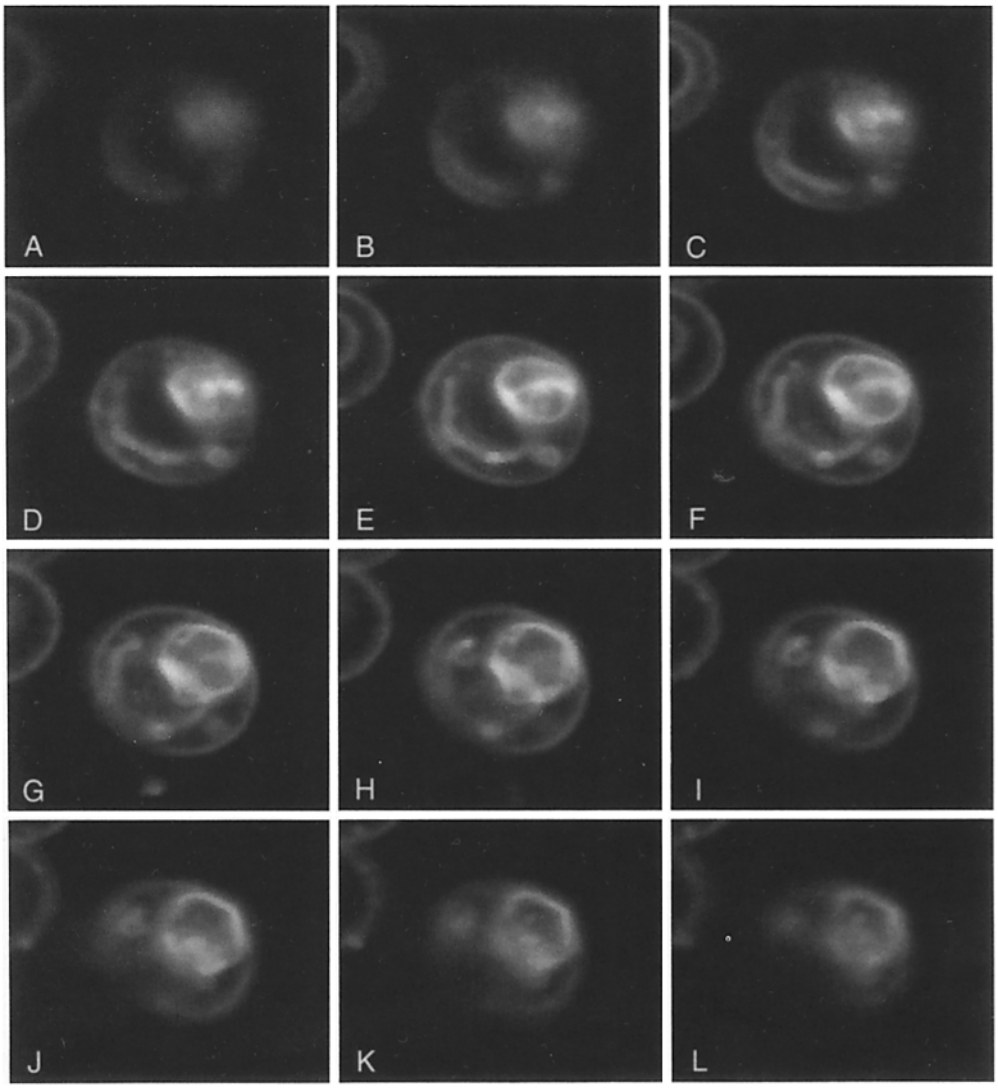

Figure 1. Serial sections through a *Plasmodium falciparum*–infected erythrocyte labeled with C_5-DMB-ceramide. Infected erythrocytes were incubated in RPMI-1640 supplemented with 2 mg/ml defatted-BSA and 20 μM C_5-DMB-ceramide for 30 min at 37°C. Cells were washed to remove unincorporated label and fixed in 0.05% glutaraldehyde. Sequential micrographs (*A–L*) were taken at 400-nm intervals along the z-axis at an excitation wavelength of 488 nm. The image depicts a single trophozoite-stage infected erythrocyte. The erythrocyte membrane is the outer circle in the figure. A single trophozoite stage parasite is the smaller, brighter circle off to the right within the erythrocyte. Note the long tubule extending outward from the surface of the parasite and the smaller vesicles attached along the length of the tubule.

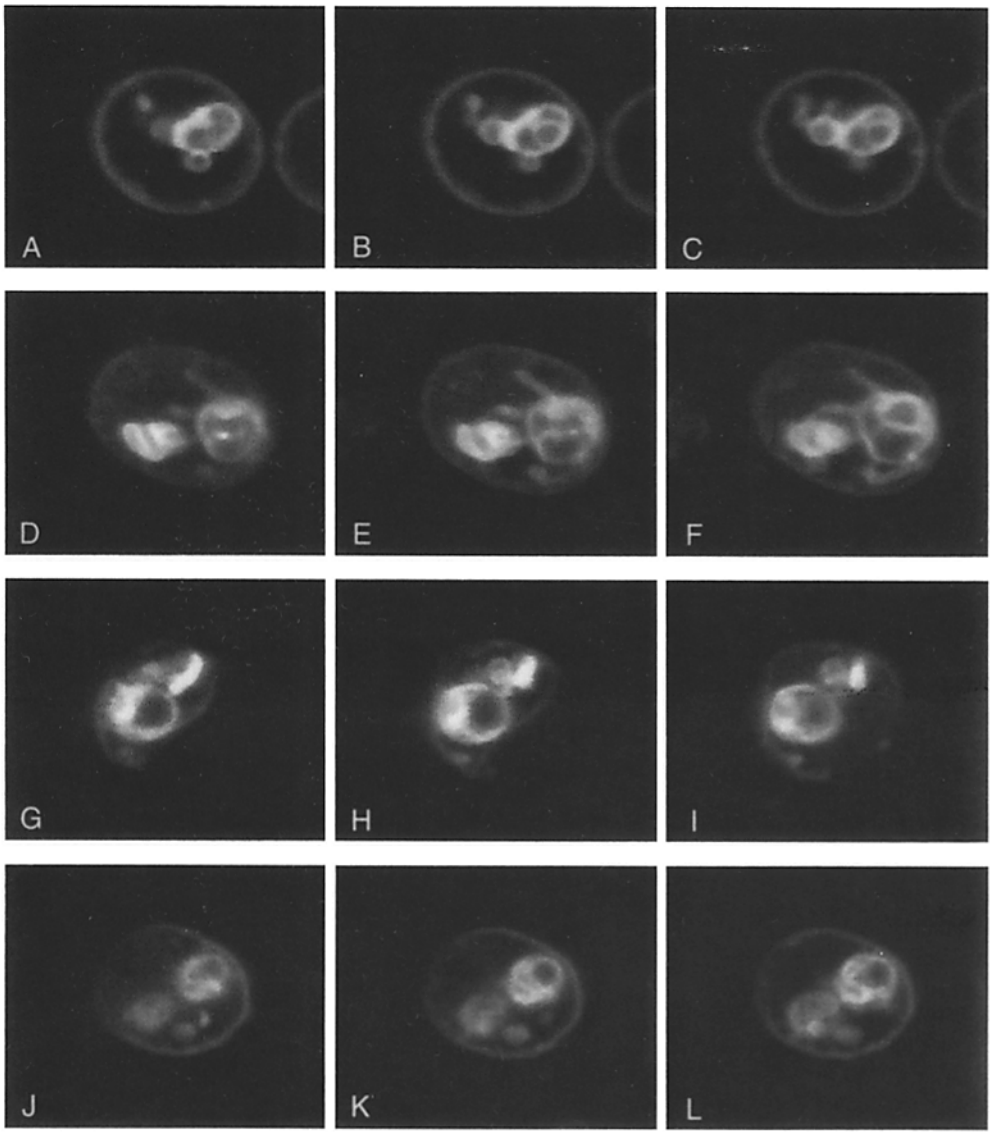

Figure 2. Serial sections through four additional *Plasmodium falciparum*-infected erythrocytes labeled with C_5-DMB-ceramide. Infected erythrocytes were labeled as in Fig. 1. The two cells shown in *A–C* and *D–F* were again fixed in 0.05% glutaraldehyde. The two cells shown in *G–I* and *J–L* were left unfixed. Sequential micrographs through the cells were taken at 400-nm intervals along the z-axis at an excitation wavelength of 488 nm. Three consecutive sections from the center of each cell are shown. In all four cells the erythrocyte membrane is the outer circle. In *A–C* the parasite is to the right within the red cell; one small projection extends at the bottom of the parasite while a series of projections extended from the left side of the parasite. In *D–F* the parasite is again to the right within the red cell; multiple projections, including one very bright and convoluted structure, protrude to the left. In *G–H* the parasite is to the left within the red cell and a very bright tubule extends up and to the right; several other smaller vesicles are seen along the length of the tubule. In *J–L* there are two parasites within the red cell; each has a small vesicle extending toward the bottom of the red cell.

tensely labeled. At the resolution of the light microscope in a cell of this size (the erythrocyte is ~7 μm in diameter, the intracellular parasite only 2–4 μm in diameter), we cannot distinguish between staining of the parasite plasma membrane and the parasitophorous vacuolar membrane; we will therefore refer to both of these membranes with the term "periphery of the parasite." The interior arc of the parasite is clearly present in Fig. 1, *E*, *F*, and *G*; this arc surrounds the nucleus of the parasite (Elmendorf and Haldar, 1993; data not shown). Many membranous structures, both tubular and vesicular, are seen in the erythrocyte cytosol. A long tubule extending away from the parasite surface toward the left side of the erythrocyte is clearly seen in Fig. 1, *B–H*; the tubule has an apparent length of ~7 μm and a diameter of <1 μm. This projection appears to connect to the labeled periphery at the bottom of the parasite in Fig. 1 *G*. Additionally, there are several large vesicles (1–2 μm diameter) projecting both from the surface of the parasite (*J* and *K*) and from the vicinity of the tubule (*D–F* and *H* and *I*). "Free" vesicles in the cytosol are not detected; consecutive images through the cell inevitably show points of attachment of these vesicles to either the parasite or to other projections, both tubules and loops.

Fig. 2 shows three consecutive sections through four additional cells. *A–C* and *D–F*, from two cells labeled and fixed as in Fig. 1, demonstrate the range of morphologies observed in the intraerythrocytic membranes. Fig. 2, *A–C* shows a late ring stage parasite. In this example, the probe labeled large vesicles in the erythrocyte cytoplasm. Again the interior arc and the periphery of the parasite are also prominently labeled. The TVM appears as a stacked or "budding" series of large vesicles (again 1–2 μm diameter); again, these vesicles are not independent but emerge from the surface of the parasite as an apparently connected or attached series. The large vesicles were typical for ring stage parasites. Fig. 2, *D–F* shows a trophozoite stage parasite. At least four separate projections, including a large and convoluted membranous structure and three finer projections (~2–3 μm in length and <1 μm in diameter), extend from the parasite surface. The convoluted membrane suggests that the tubules may fold on themselves.

To demonstrate that the observed labeling of membranes was not an artifact of the glutaraldehyde fixation, live cells were labeled and viewed (three consecutive sections through two cells are shown in Fig. 2 (*G, H, I* and *J, K, L*). Since repeated exposure of cells to a laser beam can induce pho-

todamage, care was taken to work at levels of probe and laser intensity to minimize such damage. With live cells an early indication of such damage is the swelling of the erythrocyte membrane and its subsequent lysis and release of hemoglobin. Therefore cells were viewed by bright field microscopy both before and after serial sectioning to ensure that the erythrocyte membrane was intact in cells used for analysis. Again the interior arc was visible (Fig. 2, *H* and *K*) and the peripheries of the parasites were well defined. Prominent projections of both tubules and vesicles are also detected in the sections. In Fig. 2, *J–L* the erythrocyte is doubly-infected; a connection between the parasite on the left and the lower vesicle in seen in Fig. 2 *L*, while the point of contact between the parasite on the right and the vesicle below it is seen more clearly in the next consecutive section of the series (not shown). In both fixed and live cells, regions of higher intensity labeling are detected both within the parasite and in the TVM, suggesting the presence of domains which accumulate fluorescent sphingolipids in these membranes.

Three-dimensional Reconstruction of Parasite/TVM Morphology

Using three-dimensional reconstructions of sequential confocal images, these membranes appear as a large, interconnected reticulum that extends outward from the parasite surface into the erythrocyte cytosol. 20, 400-nm serial, z-sections from the two cells shown in Fig. 1 and Fig. 2, *A–C* were used for this modeling (Figs. 3 and 4, respectively). The data set is first processed through a three-dimensional Gaussian filter (ImageSpace; Molecular Dynamics Inc., Santa Clara, CA). This will suppress continuous noise and very fine detail by using weighting factors based on a three-dimensional Gaussian distribution and applying them to a pixel and its neighboring pixels in space {[Σ(pixel value)-(weighting factor from Gaussian distribution)/Σ (weighting factors)] = new pixel value}; the filter was applied simultaneously to the entire data set. Thresholds for signal intensity were then set so as to eliminate ~95% of the signal seen on uninfected erythrocytes in the sample. The label on uninfected erythrocytes was designated as non-specific label to allow us to look only at lipid labeling properties induced by the parasite in the infected red cell. This method also allows subtraction of "bleed-through" of signal from adjacent sections along the z-axis. A three-dimensional model of the cell is then formed by linear interpolation between the "slices" of images to create three-dimensional voxels from the two-dimensional pixel data set (ImageSpace). The models were visualized using a "depth-coding" function that presents only the surface of the cell as an opaque image and colors it with respect to its distance from the viewer. The result is a model of the surface of the parasite and its projections, with the

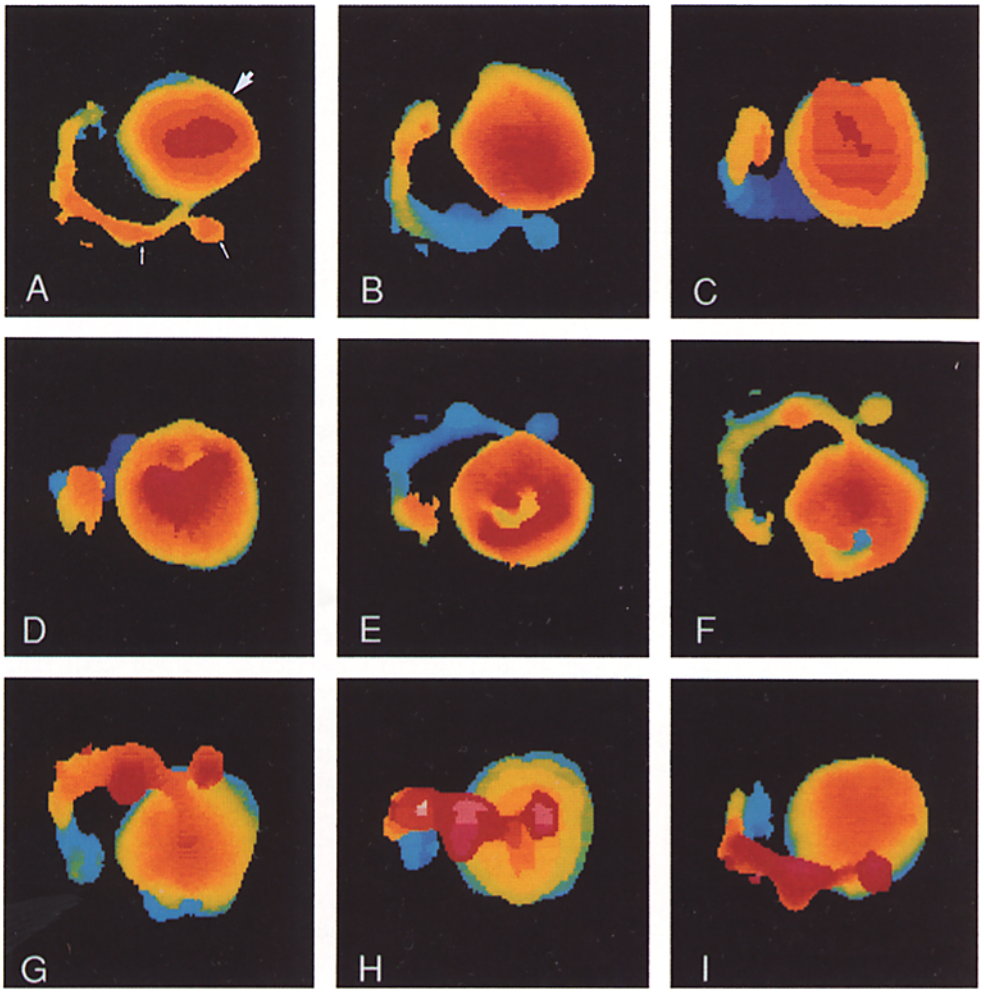

Figure 3. Three-dimensional reconstruction of the trophozoite-stage parasite shown in serial sections in Fig. 1. 20 consecutive images taken at 400-nm intervals through the depth of the infected erythrocyte were used to recalculate the three dimensional morphology of the parasite. The images were first processed through a Gaussian data filter to eliminate non-specific signal and noise, and then the image intensity threshold was set to exclude signal from uninfected erythrocytes in the same sample. Sequential images (*A–I*) are shown as the model rotates around the x-axis at 40° intervals. Colors indicate depth of image: warm colors (*reds*) are closest to the reader and cooler colors (*blues*) are furthest away. The arrowhead in *A* points to the body of the parasite, while the two smaller arrows point to the long tubule and a smaller vesicle protruding from the tubule.

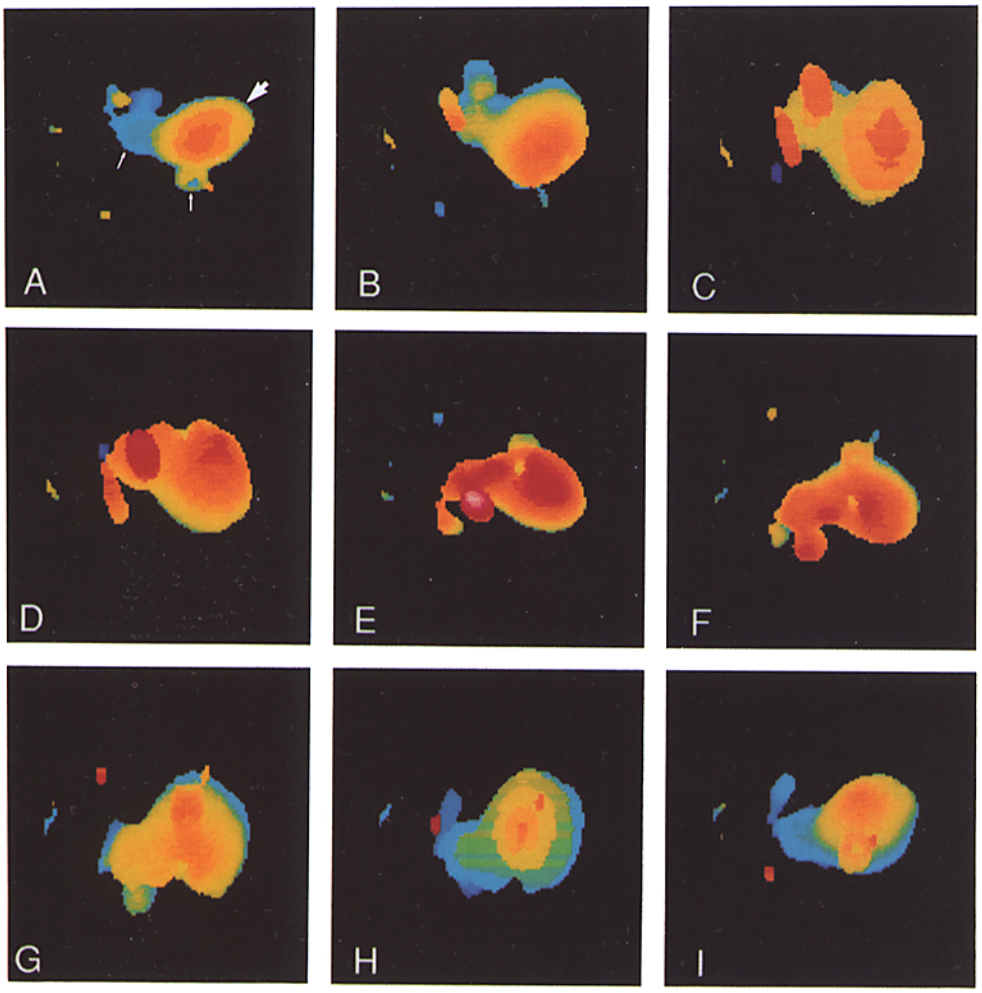

Figure 4. Three-dimensional reconstruction of the ring-stage parasite shown in serial sections in Fig. 2, *A–C*. Images were processed as described in Fig. 3. The arrowhead in panel *a* points to the body of the parasite, while the two smaller arrows point to two large vesicular structures protruding from the surface of the parasite.

more proximal part of the image highlighted in "warm" colors (*reds*) while the more distal part of the image appears in "cool" colors (*blues*). These models do not distinguish between different labeling intensities along the membranes—all signals above threshold are considered equal.

The first frame in each model shows the three-dimensional cell as it looks in the serial sections. In the next eight frames, the cells are turned around the x-axis at 40° intervals to provide a view from different perspectives. In Fig. 3 the parasite is shown as a large spherical structure in warm colors (designated by an *arrowhead*), while the tubule (designated by two *smaller arrows*) first rotates back into the page, up to the top of the page, and then out of the page. In Fig. 4 the parasite is first seen in warm colors at the right of the view (designated by an *arrowhead*), while three vesicles (designated by two *smaller arrows*), in blue, protrude in a series at the left of the parasite and a single vesicle, in green/blue, extends at the bottom of the cell. The vesicles series rotate first out of the page, down toward the bottom of the page, and then back into the page.

Many features become readily apparent from these models that are not clearly discernible in the serial images. First, the labeling intensity of the red cell membrane is much lower than the intensity of the parasite membranes. The entire confocal image is processed identically in the programs, and so the "disappearance" of a membrane denotes it as being relatively less bright. In both reconstructions, however, small sections of the red cell membrane are still visible. Similar spots are seen on uninfected cells at the same threshold and as such probably represent small variations of label on the erythrocyte membrane independent of parasite activities. Second, the true shape of the intraerythrocytic structure is restored. In the serial sections, the long "tubule" actually appears in seven consecutive sections, suggesting a "sheet" structure. However, by removing the "bleed-through" of signal along the z-axis, the membrane is resolved into much finer tubular dimensions. Third, both reconstructions strongly suggest a junction of contact between the parasite and either the tubule (Fig. 3) or the first loop (Fig. 4). Similarly there is close juxtaposition of the tubule and the smaller vesicles (in Fig. 3) and the large vesicle and its two smaller "ear-like" vesicles (in Fig. 4). Fourth, variations in the surface of the parasite are revealed. In Fig. 3 *E* and *F*, an area of yellow and then blue appears in the red–orange of the parasite, denoting a deep indentation in the surface of the parasite. While we cannot resolve its precise significance, such an indentation may represent a site of endocytosis on the parasite surface; endocytic vacuoles for the uptake of hemoglobin have been suggested based on three-dimensional modeling of transmission electron micrographs (Slomianny, 1990).

The Intraerythrocytic Membranes are a Site of Specific Sphingolipid Accumulation

The fluorescent ceramide analogues can diffuse across lipid bilayers and aqueous spaces to label all cellular membranes (Pagano, 1989). To identify specific sites of sphingolipid accumulation in infected erythrocytes, the cell associated fluorescent label was partially removed by incubating live, labeled cells with excess BSA, in a process called back-extraction. This removed excess label from cellular membranes. For these experiments the probe C_6-NBD-ceramide was used for two reasons: first, it is efficiently back-extracted (as opposed to C_5-DMB-ceramide) (Pagano et al., 1991); and second, the use of a second fluorescent moiety allowed us to confirm that the prominent staining observed with C_5-DMB-ceramide reflected sphingolipid binding and accumulation which was independent of the fluorescent tag.

Infected erythrocytes were incubated with 20 μM C_6-NBD-ceramide at 0°C, and after extensive washing, incubated at 37°C for 60 min. C_6-NBD-sphingomyelin was formed under these conditions, but the majority of the probe in the cell at this time was still present as C_6-NBD-ceramide as judged by thin-layer chromatography analysis of the fluorescent lipid species (data not shown). Cells were then back-extracted three times at 0°C in the presence of excess defatted-BSA. As previously reported (Haldar et al., 1991), we observed only removal of ceramide during back-extraction; C_6-NBD-sphingomyelin was not removed (data not shown). Consecutive serial z-sections from a cell are shown in Fig. 5. Most noticeable was the dramatic reduction of label on the infected red cell membrane and on uninfected erythrocytes. Again the periphery of the parasite, the interior arc, and the vesicles within the erythrocyte cytosol are clearly labeled. However, in this cell, as in others the apparent connections between the parasite and these vesicles are no longer visible. Therefore, membrane domains of the TVM which specifically accumulate sphingolipids, are not necessarily situated along the periphery of the parasite. It might have been possible to predict this result because, while clearly visible, the region of apparent connection is often less intensely labeled even in the non-back-extracted cells shown in Fig. 1 and Fig. 2.

Sphingomyelin Synthase in Merozoites and the Presence of the Merozoite Activity in Ring and Trophozoite-infected Red Cells

Since both C_5-DMB-ceramide and C_6-NBD-ceramide are metabolized to their sphingomyelin analogues in infected erythrocytes, we decided to directly investigate the distribution of sphingomyelin synthase activity in the malaria parasite. We have previously shown that uninfected erythrocytes contain no detectable sphingomyelin synthase activity (Haldar et al., 1991). Because no antibodies or even gene sequence are available for the enzyme, identification of sphingomyelin synthase must be performed by direct analysis of the enzymatic activity.

In the asexual cycle intraerythrocytic parasites develop from ring to trophozoite to schizont stages. Schizogony is a period of nuclear division and growth of the original parasite. It culminates in the formation of 10–16 merozoites (44–48 h after invasion) when the parasite plasma membrane pinches off around the daughter nuclei and a corresponding set of organelles. We have previously shown that in schizonts there is a perinuclear region of sphingomyelin biosynthesis around each nucleus (Elmendorf and Haldar, 1993). We also showed that when daughter merozoites form, each inherits its own perinuclear region of sphingomyelin biosynthesis, suggesting that the extracellular merozoites should contain sphingomyelin synthase. In the very late schizont stages the enzyme appears to concentrate in the perinuclear arc within the individual merozoites (Elmendorf and Haldar, 1993).

We therefore examined the presence of sphingomyelin synthase in isolated merozoites, purified and rendered completely free of other parasite stages (Mrema et al., 1982; see Materials and Methods). As shown in Table I, when equal numbers of parasites from independent preparations of isolated merozoites were incubated with either C_6-NBD-ceramide (or C_5-DMB-ceramide; data not shown), very similar amounts of fluorescent sphingomyelin were synthesized. Doubling either the time of incubation or the amount of cell material resulted in a linear increase of product formed in each reaction, confirming that the levels of sphingomyelin produced were a true measure of enzyme activity. A specific activity of 49 $\pm$ 6 pmols of C_6-NBD-sphingomyelin/min/mg protein was calculated from five independent isolated merozoite preparations, indicating the consistency of the individual preparations. (The presence of EDTA had no effect on this activity). Hemozoin, a crystalline product of parasite heme digestion, was present in varying amounts in the different preparations but appeared to have no effect on either the protein content or sphingomyelin synthase activity of the merozoite fractions. Furthermore, when preparations labeled with NBD-ceramide were examined in the microscope, prominent fluorescence was detected in the merozoites but not in association with the hemozoin crystal (not shown). These results indicate that isolated extracellular merozoites

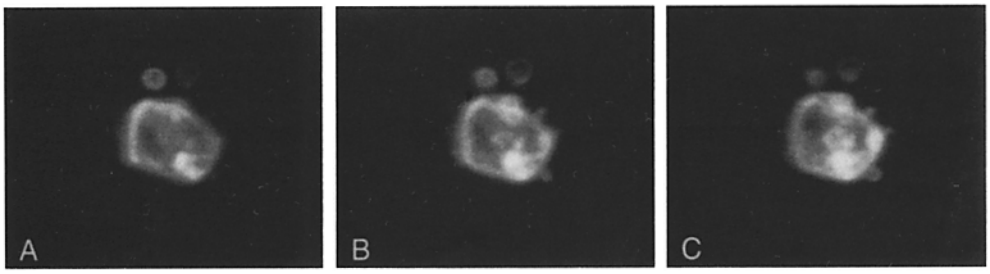

Figure 5. Sites of specific ceramide accumulation in *P. falciparum*-infected erythrocytes labeled with C_6-NBD-ceramide. Infected erythrocytes were loaded with 20 μM C_6-NBD-ceramide at 0°C, unincorporated label removed by extensive washing, and partial metabolic conversion of probe to C_6-NBD-sphingomyelin allowed to continue at 37°C. Cells were then back-extracted three times at 0°C in the presence of 7 mg/ml defatted-BSA. Visualization of cells was performed as described in Fig. 1. Three consecutive sections from the center of the cell are shown.

Table I. Analysis of NBD-Sphingomyelin Synthesis in Merozoites, Ring-, and Trophozoite-infected Erythrocytes

	Number of cells ($\times 10^8$)	pmoles of NBD-Sm 15 min	pmoles of NBD-Sm 30 min
*Merozoites (extracellular)**			
PrepI	1	7	15
PrepII	2	13	26
PrepIII	2	14	29
Intracellular stages‡			
Rings	1	7	15
	2	13	26
Trophs (<30 h)	1	8	17
	2	15	28
Schiz (>40)	1	88	188
	2	181	362
Effects of cycloheximide§			
Rings + cycloheximide	2		29
− cycloheximide	2		28
Trophs + cycloheximide	2		27
− cycloheximide	2		29
Schiz + cycloheximide	2		173
(∼36 h) − cycloheximide	2		252

* Merozoites were purified and incubated with C_6-NBD-ceramide. At the indicated times, samples were extracted and amount of C_6-NBD-sphingomyelin synthesized was determined as described in Materials and Methods.
‡ Ring- or trophozoite- and schizont-infected erythrocytes were incubated with C_6-NBD-ceramide and the samples were processed identically as above.
§ Ring or trophozoite infected erythrocytes were either pretreated with cycloheximide or mock treated as described in Materials and Methods, incubated with C_6-NBD-ceramide for 30 min and the amount of C_6-NBD-sphingomyelin was determined. The numbers shown are the average of three experiments. They have been rounded off to the closest whole number.

contain significant amounts of sphingomyelin biosynthetic activity.

As indicated earlier, subcellular fractionation studies in rat liver indicate that 87% of sphingomyelin synthase is found in the Golgi and 13% is at the plasma membrane. However, other studies suggest that higher levels of the enzyme may be at the plasma membrane. We were therefore interested in determining the relative distribution of exported versus intracellular sphingomyelin synthase in the isolated merozoites. To do this we examined the effect of exogenously added protease on the sphingomyelin synthase activity of merozoites. As shown in Table II, when proteinase K was added to intact merozoites, it had no effect on their sphingomyelin synthase activity. The presence of 0.1% wt/vol CHAPS and 1% wt/vol saponin also did not reduce levels of

Table II. Effect of Proteinase K on the Synthesis of NBD-Sphingomyelin in Merozoites

Treatment	Percent activity (NBD-Sm synthesis) after treatment
Untreated	100
Proteinase K	105
0.1% CHAPS, 1% saponin	93
0.1% CHAPS, 1% saponin, Proteinase K	18

Merozoites were isolated and purified, incubated with either 100 μg/ml proteinase K, detergent or both as indicated in Materials and Methods. The results are the average of four experiments.

enzyme detected with the merozoites; however, as previously reported (Futerman et al., 1990), detergents such as triton X-100, NP-40, deoxycholate, *n*-octylglucoside resulted in loss of activity when they effectively permeabilized the cells and therefore could not be used (data not shown). When protease and 0.1% wt/vol CHAPS/1% wt/vol saponin were added together to merozoites, an ∼80% reduction in sphingomyelin synthesis was observed. The residual activity was probably due to incomplete permeabilization of the merozoites (it was not possible to increase the levels of CHAPS and saponin since this led to a loss of activity in the absence of protease). These results indicate that all sphingomyelin synthase activity in the extracellular merozoite resides within the parasite.

In the asexual cycle, the extracellular merozoites rapidly (within minutes) re-invade red cells and form ring stage parasites. Some merozoite components are detected in rings while others are processed and discarded (Blackman et al., 1990). We found that levels of sphingomyelin synthesis are comparable in equal numbers of merozoites, rings and trophozoites (under 30 h of development; see Table I). We then investigated whether sphingomyelin synthase activity in ring and trophozoite stage infected red cells was due to de novo synthesis of sphingomyelin synthase, possibly coordinate with the degradation of merozoite activity. However, surprisingly, pretreatment of ring or trophozoite infected cells in cycloheximide for three hours (Table I) or for 5 h (data not shown) followed by incubation in cycloheximide and C_6-NBD-ceramide had no effect on the levels of sphingomyelin formed. We independently confirmed that cycloheximide blocked parasite development and protein synthesis and was therefore active in the cells (data not shown). Upon removal of the drug protein synthesis and parasite growth were quickly restored to normal levels. Sphingomyelin synthase in ring and trophozoite stage parasites is apparently not due to de novo synthesis of the enzyme in these stages but instead corresponds to that present in the entering merozoite.

At schizogony, levels of sphingomyelin synthase increase, and mature schizonts (after 40 h) contain 10–16 times more activity than ring and trophozoite stages (Table I). Pretreatment of ∼36 h schizonts with cycloheximide leads to a marked decrease in the levels of enzyme detected in the cell (Table I). Thus de novo synthesis of sphingomyelin synthase occurs during schizogony.

Export of Sphingomyelin Synthase Activity by Intracellular Ring and Trophozoite Stage Parasites

To examine the distribution of sphingomyelin synthase activity in intracellular stage parasites, we used a system we had previously developed to separate ring and trophozoite stage parasites from their red cell hosts (Elmendorf et al., 1992). The release and isolation of parasites is achieved by mechanical disruption and Percoll density centrifugation. These parasites have been denuded of the majority of their tubovesicular membrane extensions as judged by phase microscopy (Elmendorf, H. G., and K. Haldar, unpublished observations), but are intact and capable of active protein synthesis and secretion as determined by rigorous biochemical criteria (Elmendorf et al., 1992). As shown schematically in Fig. 6, by disruption of the infected erythrocyte (Fig. 6 *A*), we separated intact malaria parasites (Fig. 6 *B*) from

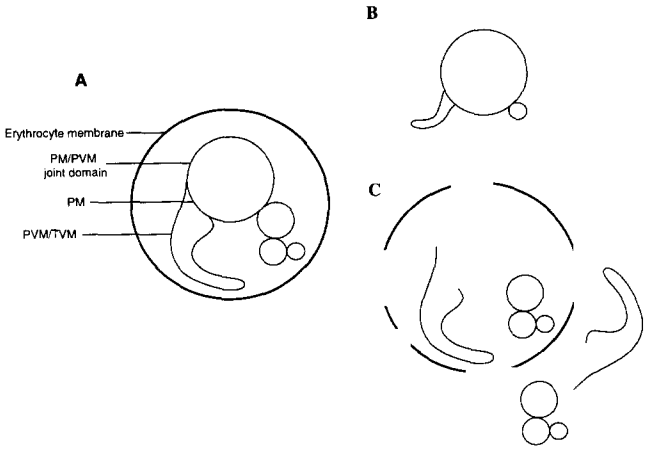

Figure 6. Fractionation of *P. falciparum*-infected erythrocytes. Infected erythrocyte (*A*). Released parasite with parasitophorous vacuolar membrane (*B*). Erythrocyte membrane (EM) and tubovesicular membrane fraction (TVM) (*C*). The TVM is found associated with the EM and also free in this fraction.

a fraction enriched in erythrocyte membranes and the tubovesicular membrane network (EM/TVM) (Fig. 6 *C*). The accumulation of fluorescent sphingolipid analogues at sites both within the parasite and in the erythrocyte cytosol suggested that the membranes of the TVM shared lipid binding properties with the Golgi membranes of mammalian cells, and we were therefore interested in the properties of the EM/TVM fraction as well. Cell equivalents of uninfected erythrocytes, infected erythrocytes, released parasites, and purified EM/TVM membranes (and where indicated erythrocyte cytosolic fractions) were used in these experiments; normalization to protein content, as is often standard for cellular fractionation studies, is not applicable in this system due to the high hemoglobin content of infected erythrocytes. Samples were incubated in 10 μM C_6-NBD-ceramide for 60 min at 37°C, and lipids extracted and analyzed for conversion to sphingomyelin.

In three independent experiments shown in Table III, an average of 51% of the original sphingomyelin synthase activity was recovered in the released parasites, while an average of 39% of the activity was in the EM/TVM fraction. The presence in the EM/TVM of a significant proportion of the total sphingomyelin synthase is consistent among twelve independent fractionations that have been performed. Together, these fractions accounted for an average of 90% of the sphingomyelin synthase activity present in the starting population of infected erythrocytes. No metabolic products other than sphingomyelin were observed. In the three representative experiments shown, released parasites contained 65, 26, and 62% of the infected erythrocyte sphingomyelin synthase activity, while the EM/TVM fraction contained the remaining 36, 52, and 29%. Based on our assessment of the specific stage of the parasites used in each of the preparations, this variation is a consequence of the age and synchrony of the parasite population (see Discussion). Although variable, these numbers suggest a redistribution of sphingomyelin synthase activity to sites beyond the parasite.

In any cellular fractionation, contamination of the different fractions is always a concern. In the homogenization procedure, a small number of parasites are disrupted, and membranes from these parasites are then presumably present in the total membrane fraction isolated on the sucrose cushion. To ensure that this small percentage of disrupted parasites did not result in the high levels of sphingomyelin synthase activity seen in the TVM fraction, we analyzed the degree of contamination from parasite lysis in two ways. First, parasite numbers were counted both before the release procedure and after the cells were pelleted from the homogenate. The difference between these counts divided by the total number of starting parasites represents the maximal percentage contamination; this calculation assumes that all disrupted parasite membranes will emerge in the EM/TVM fraction, therefore grossly overestimating the contamination of the EM/TVM. The second method used to calculate contamination was Western blot analysis of cell equivalents of the final fractions. We used antibodies against a *P. falciparum* integral membrane protein, PfERD2, as a marker for the presence of internal parasite Golgi membranes in the fractions. PfERD2 can be detected in all stages of the intraerythrocytic

Table III. Distribution, Percentage Recovery of Sphingomyelin Synthase and Parasite Markers between Released Parasites and the EM/TVM

	Sphingomyelin synthase activity			PfERD2 (Golgi)	MSP1 (plasma mb)	45 kD (intraerythrocytic cisternae)
	Percent of infected erythrocytes					
Fraction	1	2	3			
A. Infected eryth.	100	100	100	100	100	100
B. Released parasites	65	26	62	90	75	2
C. EM/TVM	36	52	29	5	17	49*
D. Erythrocyte cyto.	–	–	–	–	–	36*
E. Percent recovery *B–D*	101	78	91	95	92	87

For the sphingomyelin synthase assays, cell equivalents of fractions were incubated in buffer A supplemented with 2 mg/ml defatted-BSA and 10 μM C6-NBD-ceramide for 60 min at 37°C. Lipids were extracted and analyzed by thin layer chromatography. Spots migrating at the appropriate Rf for sphingomyelin were scraped and quantitated. The results from three typical individual experiments are shown. The kinetics of sphingomyelin production was linear over this time. For PfERD2, MSP1 and the 45-kD protein, cell equivalents of fractions were probed in Western blots with the appropriate antibody and subjected to densitometry analysis. The average of three PfERD2, six MSP1 and three 45-kD determinations are shown. The numbers have been rounded off to the closest whole number.
* The mature 45-kD protein is detected in a membrane form associated with the intraerythrocytic cisternae, as well as a solbule form in the erythrocyte cytosol (Li et al., 1991; Das, Elmendorf and Haldar, manuscript submitted for publication).

life cycle and localizes to a tight perinuclear site within the parasite (Elmendorf and Haldar, 1993). The presence of PfERD2 found in the different fractions in several different preparations was determined by densitometry analysis of Western blots; in three representative experiments 5% of PfERD2 was found in the EM/TVM fractions, and 90% in the released parasites. In contrast, a 45-kD protein which resides in cisternal membranes in the erythrocyte cytosol and is recognized by a monoclonal antibody LWLI (Li et al., 1991), is present in very low levels (2%) in the released parasites (Table III), indicating that this fraction is not contaminated by the intraerythrocytic membranes. 49% of this protein is in the EM/TVM fraction, consistent with the localization of the cisternae in the infected erythrocyte. 36% of the 45-kD protein was detected as a soluble protein in an erythrocyte cytosolic fraction generated upon homogenization of infected erythrocytes. Biosynthetic studies confirm that in trophozoite-infected erythrocytes, the mature 45-kD protein exists in both soluble and membrane associated forms (Das, Elmendorf and Haldar, in preparation). The relative distribution of PfERD2 and the 45-kD protein indicate a good separation of the EM/TVM fraction from internal parasite Golgi membranes. 17% of a plasma membrane protein, MSP1 was also found in the EM/TVM fraction. Assuming that all of the MSP1 in the EM/TVM fraction reflects contamination, we found on average 25% of the total sphingomyelin synthase activity in the EM/TVM fraction. Using the degree of contamination estimated by the cell breakage for each preparation, we found an average of 26% of the total sphingomyelin synthase activity located in the EM/TVM fraction. These numbers are very comparable and confirm the export of a significant percentage of a Golgi enzyme beyond the parasite plasma membrane. This is in contrast to the complete intracellular retention of the enzyme in merozoite stages. In particular the lack of new enzyme synthesis in these early intracellular stages implies that this exported enzyme corresponds to a form present within the merozoite. *P. falciparum* appears capable of developmentally regulated export of sphingomyelin synthase.

Discussion

We have used C_5-DMB-ceramide and C_6-NBD-ceramide to label the parasite and membranes in the erythrocyte cytoplasm in *P. falciparum*–infected cells. Both probes are extremely mobile and diffuse into all intracellular membranes. In mammalian cells both probes bind specifically in the Golgi by virtue of their ceramide moiety and are correctly metabolized and sorted (Pagano, 1990). C_5-DMB-ceramide is more photostable with a greater quantum yield (Pagano et al., 1991), and was therefore preferentially used in our microscopy studies. By high resolution laser confocal microscopy the morphologies of membranes which concentrated C_5-DMB-ceramide were found to be identical to those which concentrated C_6-NBD-ceramide. Hence, fluorescence accumulation should accurately reflect sphingolipid accumulation in infected erythrocytes.

Organization of the TVM with Respect to the Parasite Surface and the Erythrocyte Membrane

Scanning electron micrographs by Elford and Ferguson

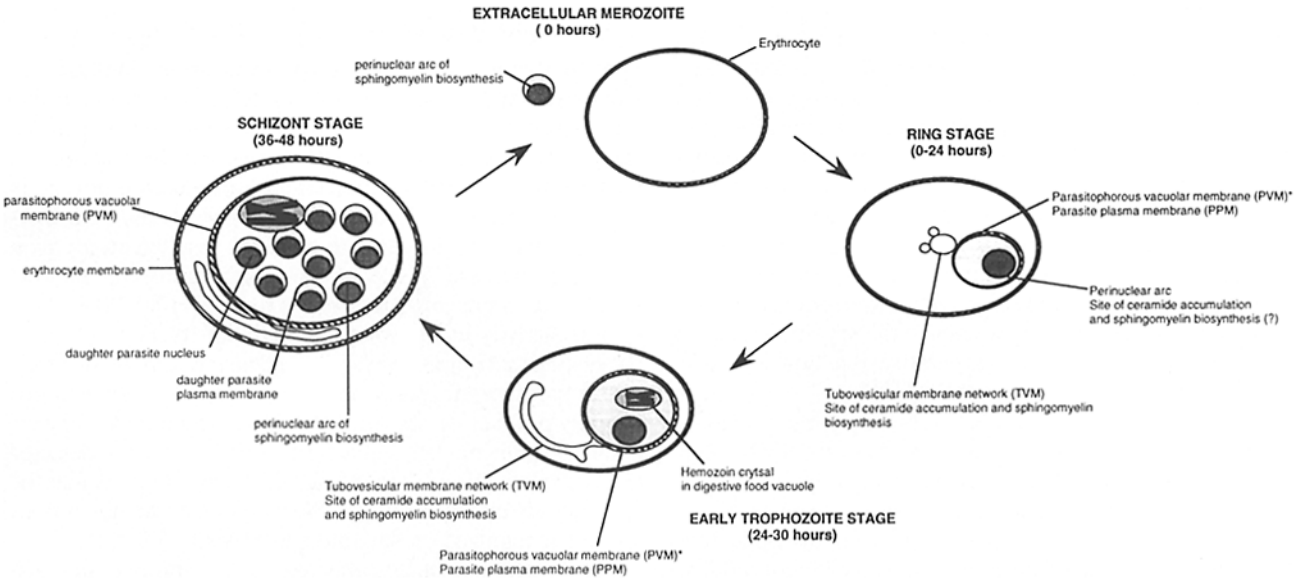

Figure 7. Model for the stage-specific regulation of sphingomyelin synthase activity. The life cycle of *P. falciparum* is shown starting at the left with the mature schizont stage. After the cycle in a clockwise direction, merozoites are released and re-invade new erythrocytes. During the merozoite stage the enzyme is localized within the parasite in a perinuclear arc. After invasion, the parasite matures into ring and then trophozoite stages. (*) It is not possible to distinguish between sphingolipid staining of membrane from the parasitophorous vacuolar membrane and the parasite plasma membrane at the ring and trophozoite stages. Here the parasite induces the development of a tubovesicular network beyond its plasma membrane and exports the sphingomyelin synthase enzyme, originally present solely within the merozoite, partially outward into these membranes. The cycle is completed with the maturation of the parasite into the mitotically dividing schizont stage. As expected the parasite appears to replicate sphingomyelin synthase as it divides, resulting in enzyme levels increased 10–15-fold in the schizont stages compared with the earlier intracellular stages (Table I).

(1993) indicated the presence of long continuous tubovesicular elements extending from the surface of parasites released from their host cell membranes. Here we show that a similar morphology can be seen in tubovesicular membranes in the erythrocyte cytosol of intact infected erythrocytes. One end of the TVM is closely juxtaposed to the parasite's surface as indicated schematically in Fig. 7; however, at the level of resolution possible with the confocal microscope, we are unable to determine whether this area of juxtaposition unambiguously represents a continuum of lipid bilayers. We also define a specific site of lipid accumulation within the ring and trophozoite parasites in the form of a perinuclear arc. By analogy with our results in schizont-infected erythrocytes (Elmendorf and Haldar, 1993) this arc is likely to be a site of sphingomyelin biosynthesis in these younger stage parasites. In future studies it will be interesting to investigate trafficking pathways between the apparent region of contact of the TVM with the parasite's periphery and the perinuclear region of sphingolipid labeling in the parasite.

Previous studies by our lab demonstrated that two parasites within the same host erythrocyte will each export lipids to their own TVM during parasite development, but, surprisingly, the two parasites do not exchange lipids (Haldar and Uyetake, 1992). This then brings into question how material is transported from the parasite to these membranes with such precision. A direct connection between the parasite and the TVM could allow protein and lipid export to the TVM without need for the formation of discrete vesicular intermediates in the intraerythrocytic cytosol or the ability of the vesicles to distinguish between the two TVM. In this context it is interesting to note that using heterologous antibodies we have been unable to detect the presence of the β-COP, clathrins, or adaptins in association with the intraerythrocytic structures (W-l. Li, H. Elmendorf, and K. Haldar, unpublished data). It is possible that the antibodies used may not cross react with homologous *Plasmodium* proteins, but they are found to be widely cross reactive across cell types. This suggests that the two well defined mechanisms of vesiculation are not induced in the infected erythrocyte cytosol. Instead what is observed is a mechanism of membrane movement in specific domains at the parasite's surface. This initiates a membrane bud, which does not dissociate as a transport intermediate from the parent membrane, but continues to grow. It is further possible that such movement is the first step in the export of parasite proteins to the erythrocyte, and requires their transport across a putative junction for trafficking between the parasite and the TVM.

Levels of the sphingolipid label in the erythrocyte membrane were very low compared with levels in the TVM, the parasite periphery, or the perinuclear arc. In cells labeled with C_6-NBD-ceramide, back-extraction depletes label at the erythrocyte membrane. These results confirm that the red cell membrane is not a prominent site of sphingolipid accumulation in these cells. They also suggest that the lipid bilayer of the TVM is not in continuum with the erythrocyte membrane. The tight apposition often seen between the TVM and the erythrocyte membrane (clearly shown in Fig. 1) alternately suggests that the TVM interacts with the cytoplasmic face of the erythrocyte membrane, possibly its cytoskeleton, and these interactions may well contribute to the morphology of the TVM. Mechanical homogenization of *Plasmodium*-infected erythrocytes releases the parasites, but the TVM remains in association with the red cell membrane, consistent with a tight interaction between the two membranes.

Stasis of the TVM Complex

As can be seen in Fig. 2, *G–H* and *I–K*, consecutive images of live cells taken at four second intervals show no detectable movement of the intraerythrocytic membranes, and the same organization of tubovesicular morphology was observed in two consecutive z-series of sections (each lasting 1.5 min; data not shown). Further, no movement was observed on repeated imaging in a single confocal plane at intervals of 2 to 10 s (data not shown). Rapid movement of the membranes was observed only if the erythrocyte membrane had lysed or was swelling in the process of lysis. In recently or incompletely lysed cells, only the TVM showed movement; in completely lysed cells, even the body of the parasite shifted its position. In contrast, Gormley et al. (1992) used C_6-NBD-phosphatidyl choline and C_6-NBD-phosphatidyl ethanolamine to detect rapidly moving membrane vesicles in the erythrocyte cytosol. However, this movement was neither temperature nor energy dependent, and hence its significance in membrane transport is unclear. Although we consider it unlikely, it is formally possible that the sphingolipid probes do not label the vesicles detected with the phospholipid probes. It is of course expected that the membranes of the TVM move/extend during their biogenesis, but in a short time course neither the tubular structures nor the large loops altered either their position or their morphology. It remains to be seen whether submicron particles, analogous to those detected in the Golgi in mammalian cells (Cooper et al., 1990), are transported between elements of the TVM.

Distribution of Sphingomyelin Synthase

Sphingomyelin synthase is a membrane enzyme and its substrates are lipids, making it difficult to accurately determine their concentrations in the bilayer. Therefore, to correctly assay for the enzyme activity, we carried out the reactions in an excess of C_6-NBD-ceramide and over a period of time in which the kinetics of product formation were linear. Furthermore an increase in parasite material resulted in a corresponding increase in the levels of sphingomyelin product formed. We were consistently able to recover 80–90% of the original activity in the isolated subcellular fractions, strongly suggesting that our assay was also a true measure of the levels of the parasite enzyme in these experiments. Interestingly, the only product we see from extended incubations with ceramide is sphingomyelin—glycosyl ceramides are not detected (Haldar et al., 1991; data not shown). This suggests that the enzymes are either missing in *Plasmodium* or that the probes are not recognized as suitable substrates.

For intracellular stage parasites, the variability in the relative distribution of sphingomyelin synthase activity between the two fractions (released parasite and EM/TVM) likely reflects the range of parasite stages in the cell populations used for the different experiments. Despite frequent synchronization of parasite development in the infected erythrocyte cultures, it is difficult to maintain good synchrony at the high parasitemias required for these experiments; the age of parasites used, therefore, ranged from 24–36 h after invasion. It is well-established that synthesis and distribution of

proteins change within this range of parasite stages (Howard et al., 1987*a*). The morphology of the parasite also changes dramatically as the parasite enlarges and the TVM alters from a vesicular to a more tubular conformation. These differences suggest either that the enzyme distribution may vary during ring and trophozoite parasite development, or alternatively, that the homogenization procedure might differentially disrupt the TVM–parasite connection at different developmental stages. Analysis of the many separate fractionations performed suggest that a greater percentage of the total activity is exported in the trophozoite stage parasites. Our fractionation studies do not distinguish between export of sphingomyelin synthase to the TVM and the erythrocyte membrane. However, these data, taken in conjunction with our microscopy data showing prominent sites of sphingolipid accumulation in the TVM but not the EM, lead us to propose that the enzyme is exported only to the TVM network.

In mammalian cells sphingomyelin synthase is concentrated in the Golgi. A small fraction also appears to be in the plasma membrane. We have previously shown that in schizonts of *P. falciparum*, there are prominent sites of sphingomyelin biosynthetic activity in the perinuclear region, consistent with its localization in the Golgi in the parasite. We now show that while in extracellular merozoites sphingomyelin synthase activity is retained within the parasite, exported activity is detected in the subsequent intracellular ring and trophozoite stages. The amount of enzyme exported by the parasite to the TVM is far greater than the fraction of the sphingomyelin synthase activity exported to the plasma membrane in rat liver. Hence in this lower eukaryote, the relative distribution of the Golgi and exported forms appears to be dependent on the cell cycle, as summarized schematically in Fig. 7. Because there is no new synthesis of sphingomyelin synthase at the ring and early trophozoite stages, it also suggests that sphingomyelin biosynthetic activity might be ascribed to one protein, whose export is mediated by a developmental reorganization the parasite's Golgi between the merozoites and ring stage cells. However, it is still formally possible that there are two forms of the enzyme residing in distinct compartments within the merozoite, only one of which exported in rings.

Possible Roles for Sphingomyelin Synthase in the TVM

The development of membranes in the erythrocyte cytoplasm has been thought to be due to their vesicular or tubular budding from the parasite's surface. Yet as discussed earlier, known mechanisms of vesiculation have not yet been detected in the erythrocyte cytosol. The asymmetric distribution of sphingomyelin and phosphatidylcholine proposed for the Golgi apparatus in mammalian cells (sphingomyelin, inner leaflet; phosphatidylcholine, outer leaflet) is also thought to force the Golgi into flattened cisternae and eventually to bud (Sheetz and Singer, 1974; Pagano, 1988). Hence, the export of sphingomyelin synthase and the synthesis of sphingomyelin on the inner leaflet of the TVM, if coupled to similarly asymmetric accumulation of a second lipid species at the outer leaflet, may provide a mechanism for the budding of membrane in this system, possibly independent of coat formation. Changes in the relative content of various lipid species in the TVM at different stages of the parasite life cycle may also affect the stage-dependent morphology of the TVM – the correlation seen between ring stage parasites and large vesicular compartments and between trophozoite stage parasites and the long tubular compartments.

Sphingolipid domains appear to modulate protein and lipid sorting in mammalian cells (van Meer, 1989; Pagano, 1990; Brown and Rose, 1992). The TVM has been implicated in the uptake of essential extracellular lipids (Grellier et al., 1991). We find it contains specific sites of sphingolipid accumulation which strongly suggests that it can sustain membrane domains which sort lipids in the bilayer. By analogy sphingomyelin accumulation in the TVM may provide mechanisms for the sorting of exported proteins between cisternae and large vesicles. The function of the TVM in sorting and targetting proteins to the erythrocyte membrane remains unresolved. Newly synthesized sphingomyelin is not exported to the red cell surface (Haldar et al., 1991), but alternative trafficking pathways could exist and need to be further investigated.

The morphological similarity of the TVM cisternae as seen by transmission electron microscopy to the Golgi cisternae of mammalian cells, and a perceived need by the parasite for transport functions beyond its plasma membrane, led to early speculation that the TVM might function as a "trafficking organelle" in the erythrocyte (Howard et al., 1987*a*). However, no biochemical function could be ascribed to these membranes. Our evidence for the export of sphingomyelin synthase is the first to indicate the presence of a Golgi activity in these membranes. The rearrangement of sphingomyelin synthase is of particular interest when compared with the retention of a *P. falciparum* homologue of ERD2, a second protein of the mammalian *cis*-Golgi, within a perinuclear locus within the parasite (Elmendorf and Haldar, 1993). The separation by the malaria parasite of these two Golgi activities (presumed to be contained within overlapping compartments of mammalian cells) suggests that the TVM cannot be considered to be simply a second "misplaced" parasite Golgi. The parasite instead elaborates a unique organelle, endowed as we have shown here with at least one Golgi-like characteristic in its lipid-processing capabilities, but perhaps more limited in various other classical Golgi functions.

We would like to thank the Cell Sciences Imaging Facility in the Beckman Center Program in Molecular and Genetic Medicine at Stanford University for advice on confocal imaging, in particular we gratefully acknowledge the help of M. Feinstein and Dr. S. J. Smith. We thank W. Jung for help on computer modeling. We are deeply grateful to Dr. M. Blackman at the National Institute of Medical Research, London for instruction in the production of merozoites and providing the initial merozoite preparation. MSP1 antibody was obtained from Dr. A. A. Holder. We thank Drs. A. A. Holder, J. Boothroyd, and S. J. Smith for encouragement during the course of this work and for careful reading of the manuscript.

This work was supported in part by grants from the National Institutes of Health (NIH) (AI26670), the MacArthur Foundation, and the Biomedical Research Support Grant RR05353 awarded by the Biomedical Research Support Program, Division of Research Resources, NIH. H. G. Elmendorf was supported in part by a National Science Foundation Graduate Research Fellowship and the MacArthur Foundation.

Received for publication 26 July 1993 and in revised form 17 November 1993.

References

Atkinson, C. T., and M. Aikawa. 1990. Ultrastructure of malaria-infected erythrocytes. *Blood Cells.* 16:351–368.

Barnwell, J. W. 1990. Vesicle-mediated transport of membrane and proteins in malaria-infected erythrocytes. *Blood Cells.* 16:379–395.

Blackman, M. J., H. G. Heidrich, S. Donachie, J. S. McBride, and A. A. Holder. 1990. A single fragment of a malaria merozoite surface protein remains on the parasite during red cell invasion and is the target of invasion-inhibiting antibodies. *J. Exp. Med.* 172:379–382.

Bligh, E. G., and W. J. Dyer. 1959. A rapid method of total lipid extraction and purification. *Can. J. Biochem. Physiol.* 37:911–917.

Brown, D. A., and J. K. Rose. 1992. Sorting of GPI-anchored proteins to glycolipid-enriched membrane subdomains during transport to the apical cell surface. *Cell.* 68:533–544.

Cooper, M. S., A. H. Cornell-Bell, A. Chernjavsky, J. W. Dani, and S. J. Smith. 1990. Tubulovesicular processes emerge from trans-Golgi cisternae, extend along microtubules, and interlink adjacent trans-Golgi elements into a reticulum. *Cell.* 61:135–145.

Coppel, R. L., J. G. Culvenor, A. E. Bianco, P. E. Crewther, H. D. Stahl, G. V. Brown, R. F. Anders, and D. J. Kemp. 1986. Variable antigen associated with the surface of erythrocytes infected with mature stages of *Plasmodium falciparum*. *Mol. Biochem. Parasitol.* 20:265–277.

Dieckmann-Schuppert, A., S. Bender, M. Odenthal-Schnittler, E. Bause, and R. T. Schwarz. 1992. Apparent lack of N-glycosylation in the sexual stage of *Plasmodium falciparum*. *Eur. J. Biochem.* 205:815–821.

Elford, B. C., and D. J. P. Ferguson. 1993. Secretory processes in *Plasmodium*. *Parasitol. Today.* 9:80–81.

Elmendorf, H. G., and K. Haldar. 1993. Identification and localization of ERD2 in the malaria parasite *Plasmodium falciparum*: separation from sites of sphingomyelin synthesis and implications for organization of the Golgi. *EMBO (Eur. Mol. Biol. Organ.) J.* 12:4763–4773.

Elmendorf, H. G., J. D. Bangs, and K. Haldar. 1992. Synthesis and secretion of proteins by released malarial parasites. *Mol. Biochem. Parasitol.* 52: 215–230.

Etzion, Z., and M. Perkins. 1989. Localization of a parasite-encoded protein to erythrocyte cytoplasmic vesicles of *Plasmodium falciparum*-infected cells. *Eur. J. Cell Biol.* 48:174–179.

Futerman, A. H., B. Stieger, A. L. Hubbard, and R. E. Pagano. 1990. Sphingomyelin synthesis in rat liver occurs predominantly at the *cis* and *medial* cisternae of the Golgi apparatus. *J. Biol. Chem.* 265:8650–8657.

Gormley, J. A., R. J. Howard, and T. F. Taraschi. 1992. Trafficking of malarial proteins to the host cell cytoplasm and erythrocyte surface membrane involves multiple pathways. *J. Cell Biol.* 119:1481–1495.

Grellier, P., D. Rigomier, V. Clavey, J-C. Fruchart, and J. Schrevel. 1991. Lipid traffic between high-density lipoproteins and *Plasmodium falciparum*-infected red blood cells. *J. Cell Biol.* 112:267–277.

Haldar, K., and L. Uyetake. 1992. The movement of fluorescent endocytic tracers in *P. falciparum*-infected erythrocytes. *Mol. Biochem. Parasitol.* 50:161–178.

Haldar, K., M. A. J. Ferguson, and G. A. M. Cross. 1985. Acylation of a *Plasmodium falciparum* merozoite surface antigen via sn-1,2-diacylglycerol. *J. Biol. Chem.* 260:4969–4974.

Haldar, K., L. Uyetake, N. Ghori, H. G. Elmendorf, and W-L. Li. 1991. The accumulation and metabolism of a fluorescent ceramide derivative in *Plasmodium falciparum*-infected erythrocytes. *Mol. Biochem. Parasitol.* 49: 143–156.

Howard, R. J., S. Uni, J. A. Lyon, D. W. Taylor, W. Daniel, and M. Aikawa. 1987*a*. Export of *Plasmodium falciparum* proteins to the host erythrocyte membrane: special problems of protein trafficking and topogenesis. *In* Host-Parasite Cellular and Molecular Interactions. K. P. Chang and D. Snary, editors. Springer-Verlag/Berlin, Germany. 281–296.

Howard, R. J., J. A. Lyon, S. Uni, A. J. Saul, S. B. Aley, F. Klotz, L. J. Panton, J. A. Sherwood, K. Marsh, M. Aikawa, and E. P. Rock. 1987*b*. Transport of an Mr~300,000 *Plasmodium falciparum* protein (Pf EMP 2) from the intraerythrocytic asexual parasite to the cytoplasmic face of the host cell membrane. *J. Cell Biol.* 104:1269–1280.

Hui, G. S. N. and W. A. Siddiqui. 1988. Characterization of a *Plasmodium falciparum* polypeptide associated with membrane vesicles in the infected erythrocytes. *Mol. Biochem. Parasitol.* 29:283–293.

Jeckel, D., A. Karrenbauer, R. Birk, R. R. Schmidt, and F. Wieland. 1990. Sphingomyelin is synthesized in the *cis* Golgi. *FEBS (Fed. Eur. Biochem. Soc.) Letters.* 261:155–147.

Kallen, K. J., P. Quinn, and D. Allan. 1993. Monensin inhibits synthesis of plasma membrane sphingomyelin by blocking transport of ceramide through the Golgi: evidence for two sites of sphingomyelin synthesis in BHK cells. *Biochim. Biophys. Acta.* 1166:305–308.

Koval, M., and R. E. Pagano. 1991. Intracellular transport and metabolism of sphingomyelin. *Biochim. Biophys. Acta.* 1082:113–125.

Langreth, S. G., J. B. Jensen, R. T. Reese, and W. Trager. 1978. Fine structure of human malaria *in vitro*. *J. Protozool.* 25:443–452.

Li, W.-l., A. Das, J-y. Song, J. L. Crary, and K. Haldar. 1991. Stage-specific expression of plasmodial proteins containing an antigenic marker of the intraerythrocytic cisternae. *Mol. Biochem. Parasitol.* 49:157–168.

Lipsky, N. G, and R. E. Pagano. 1985. Intracellular translocation of fluorescent sphingolipids in cultured fibroblasts: endogenously synthesized sphingomyelin and glucocerebroside analogues pass through the Golgi apparatus en route to the plasma membrane. *J. Cell Biol.* 100:27–34.

Mrema, J. E. K., S. G. Langreth, R. C. Jost, K. H. Rieckmann, and H. G. Heidrich. 1982. *Plasmodium falciparum*: isolation and purification of spontaneously released merozoites by nylon membrane sieves. *Exp. Parasitol.* 54:285–295.

Pagano, R. E. 1988. What is the fate of diacylglycerol produced at the Golgi apparatus? *TIBS (Trends Biochem. Sci.).* 13:202–205.

Pagano, R. E. 1989. A fluorescent derivative of ceramide: physical properties and use in studying the Golgi apparatus of animal cells. *Methods Cell Biol.* 29:75–85.

Pagano, R. E. 1990. Lipid traffic in eukaryotic cells: mechanisms for intracellular transport and organelle-specific enrichment of lipids. *Curr. Opin. Cell Biol.* 2:652–663.

Pagano, R. E., O. C. Martin, H. C. Kang, and R. P. Haugland. 1991. A novel fluorescent ceramide analogue for studying membrane traffic in animal cells: accumulation at the Golgi apparatus results in altered spectral properties of the sphingolipid precursor. *J. Cell Biol.* 113:1267–1279.

Pouvelle, B., R. Spiegel, L. Hsiao, R. J. Howard, R. L. Morris, A. P. Thomas, and T. F. Taraschi. 1991. Direct access to serum macromolecules by intraerythrocytic malaria parasites. *Nature (Lond.).* 353:73–75.

Quinn, P., and D. Allan. 1992. Two separate pools of sphingomyelin in BHK cells. *Biochim. Biophys. Acta.* 1124:95–100.

Rosenwald, A. G., C. E. Machamer, and R. E. Pagano. 1992. Effects of a sphingolipid synthesis inhibitor on membrane transport through the secretory pathway. *Biochemistry.* 31:3581–3590.

Schauer, R., M. Wember, and R. J. Howard. 1984. Sorting of malarial antigens into vesicular compartments within the host cell cytoplasm as demonstrated by immunoelectron microscopy. *Hoppe-Seyler's Z. Physiol. Chem.* 365: 185–194.

Sheetz, M. P., and S. J. Singer. 1974. Biological membranes as bilayer couples. A molecular mechanism of drug-erythrocyte interactions. *Proc. Natl. Acad. Sci. USA.* 71:4457–4461.

Slomianny, C. 1990. Three-dimensional reconstruction of the feeding process of the malaria parasite. *Blood Cells.* 16:369–378.

Stenzel, D. J., and U. A. Kara. 1989. Sorting of malarial antigens into vesicular compartments within the host cell cytoplasm as demonstrated by immunoelectron microscopy. *Eur. J. Cell. Biol.* 49:311–318.

Taylor, D. W., M. Parra, G. B. Chapman, M. E. Stearns, J. Rener, M. Aikawa, S. Uni, S. B. Aley, L. J. Panton, and R. J. Howard. 1987. Localization of *Plasmodium falciparum* histidine-rich protein 1 in the erythrocyte skeleton under knobs. *Mol. Biochem. Parasitol.* 25:165–174.

Trager, W., M. Tershakovec, L. Lyandvert, H. Stanley, N. Lanners, and E. Gubert. 1981. Clones of the malaria parasite *Plasmodium falciparum* obtained by microscopic selection: their characterization with regard to knobs, chloroquine sensitivity, and formation of gametocytes. *Proc. Natl. Acad. Sci. USA.* 78:6527–6530.

Trager, W., and J. B. Jensen. 1976. Human malaria in continuous culture. *Science (Wash. DC).* 193:673–675.

van Meer, G. 1989. Lipid traffic in animal cells. *Annu. Rev. Cell Biol.* 5:247–275.